# Decentralized Control Coordination of PV-BSS Systems in Islanded DC Nanogrids

Jimiao Zhang, Jie Li Department of Electrical and Computer Engineering Rowan University Glassboro, NJ, USA zhangj52@students.rowan.edu, lijie@rowan.edu

Abstract—Solar photovoltaics (PVs) and battery storage systems (BSSs) are two important distributed energy resources that can bring measurable environmental and economic benefits to the power grids. In this paper, a decentralized strategy is presented for coordinating the control of PVs and BSSs in islanded DC nanogrids. Depending on the measured DC bus voltages, PVs can adaptively switch between the V-P droop mode and the maximum power point tracking (MPPT) mode, thus reducing the impact of transient disturbances on the system operation. In addition, the dual active bridge (DAB) DC-DC converters are employed to interface BSSs to the nanogrid due to the converter's high-performance power conversion capabilities. To prevent overcharging/discharging of batteries, a state of charge (SoC)based adaptive droop control method is proposed. The control of PVs and BSSs is coordinated in a communication-less fashion to maintain the nanogrid load balancing, as well as to regulate the common DC bus voltage. The proposed control strategy is easy to implement with reduced complexity, while its satisfactory dynamic performance is demonstrated via numerical simulations using MATLAB/Simulink.

Keywords—DC nanogrid, state of charge (SoC), battery storage systems (BSSs), photovoltaics (PVs), dual active bridge (DAB), droop control.

## I. INTRODUCTION

A nanogrid is defined as a localized self-sustained low-voltage power system at a residential/commercial power level (typically less than 50 kW) [1-2]. A network of nanogrids can be aggregated to constitute a larger scale microgrid in a bottom-up manner. Compared with their AC counterparts, the DC nanogrids are gathering momentum in that they can achieve higher efficiency due to the absence of DC-AC or AC-DC conversion stages. Also, a DC nanogrid enables simpler system control because only voltage control is required. No reactive power control or frequency synchronization needs to be considered. With the increased deployment of rooftop solar photovoltaics (PVs), electric vehicles (EVs), and other DC appliances, DC nanogrids are regarded as one of the future electricity delivery solutions and the building block of larger scale community grids.

In the grid-connected mode, the common DC bus voltage of a DC nanogrid is maintained by an external grid through a bidirectional power converter [3]. However, DC nanogrids are still expected to operate reliably in the islanded mode, i.e., when the external grid becomes unavailable. This feature is highly desired particularly for residences during the COVID-19 Pandemic, since power outages can cause considerable economic losses as more corporate offices are shifting to homes. In addition, there has been a growing trend to deliver reliable, clean, and affordable electricity only using PVs plus battery storage systems (BSSs) [4]. Conventionally, in a nanogrid with only PVs and BSSs, the PV systems operate in the maximum power point tracking (MPPT) mode for the maximum utilization of solar energy, while BSSs are in charge of regulating the common DC bus voltage [5]. However, given the increasing penetration of PVs and the limited state of charge (SoC) of BSSs, DC bus overvoltage and BSS overcharging are likely to occur in islanded nanogrids. Thus, coordinating the control strategies of PVs and BSSs becomes critical to maintaining the common DC bus voltage and the power balance.

There has been extensive research in operating the PVs in a power-limiting mode such that they can regulate the common DC bus voltage along with BSSs [6-7]. Nevertheless, these control methods rely heavily on the communications links that are dedicated to transmission of load and/or SoC information for a smooth control mode switching, thus decreasing the system reliability with potential communication failure. For this reason, communication-less decentralized control methods have been favored for PV-BSS coordination [8-9]. In [10], cooperative adaptive droop is employed for BSSs to design a unified energy management system to optimize the battery lifespan. However, the criteria for operating mode switching are complicated, and the control performance is limited between switches due to the transient disturbances. The  $v - \frac{dp}{dv}$  droop method [11-12] senses the DC bus voltage and integrates MPPT and DC bus voltage regulation into a single control configuration. However, this scheme may suffer from slow transient responses in the case of a sudden change in environmental conditions because it utilizes a fixed PV voltage step. To this end, [13] presents a  $v - \frac{dp}{di}$ droop strategy with improved dynamic responses and power quality. But as with [11], this technique necessitates accurate measurements, and differentiation of the PV mathematical model may render the control set-points highly inaccurate in practice. A proportional droop index algorithm is reported in [14] to adjust the droop coefficient of a PV system, yet it still requires real-time measurement of each load demand to

implement the operating mode switching. A PV-BSS coordinated control method is proposed in [15], where an SoC-based droop control allows the BSSs to provide DC bus voltage regulation with balanced SoCs. Nonetheless, over-discharging protection of BSSs is not considered. Reviewing the current literature, most of this line of work either rely heavily on the reliable communication links or on the complicated mode switching criteria which are hard to implement in practice.

In order to address the above drawbacks, this work proposes a fully decentralized strategy for coordinating the control of PVs and BSSs in islanded DC nanogrids, which divides the permissible range of the common DC bus voltage into several subintervals and operates PV units and BSS units based on the measured DC bus voltages. The major contributions of this work are summarized as below:

- 1. An adaptive *V-P* control is proposed for the PVs to switch seamlessly between the droop and the MPPT modes with good dynamic response. When the DC bus voltage is higher than the preset high voltage threshold, the PVs follow the droop curve and limit the power outputs, thus participating in DC voltage regulation. If the DC bus voltage decreases below this threshold, PVs will adaptively switch to the MPPT mode to provide full power support.
- 2. The BSS units are interfaced by dual active bridge (DAB) DC-DC converters for galvanically isolated high-power conversion and operate on the proposed SoC-based adaptive droop control technique, which can mitigate overcharging and over-discharging of the batteries by adaptively adjusting the DC bus voltage references.
- 3. The proposed overall control method allows enhanced voltage regulation and power sharing among PVs and BSSs in a plug-and-play fashion, without the need to measure individual system loads.

The remainder of this paper is structured as follows: Section II elaborates the proposed overall control strategy, where adaptive controls of the PV and BSS units are also introduced, respectively. The simulation results are presented in Section III. Finally, concluding remarks and future work are provided in Section IV.

### II. PROPOSED DECENTRALIZED CONTROL STRATEGY

The proposed overall control method intends to coordinate the PVs and BSSs only through local bus voltage measurements, thereby obviating the need for communications. The concept of the DC bus voltage regulation is based on droop control. The *V-P* droop characteristics for the PV and BSS units are illustrated in Fig. 1.

 $v_{DC}^{**}$  is the nominal voltage of the common DC bus, while  $\left[v_{DC}^{\min}, v_{DC}^{\max}\right]$  is the permissible range of the common DC bus voltage. When the DC bus voltage is high enough (in the range from the high voltage threshold  $v_{DC}^{H}$  to  $v_{DC}^{\max}$ ), the PV units are supposed to limit their power outputs and operate in the droop mode. Meanwhile, the batteries should absorb excess PV generation to bring down the DC bus voltage. Under this

operating condition, PVs and BSSs maintain the power balance and regulate the common DC bus voltage together. However, when the DC bus voltage drops below  $v_{DC}^H$ , the PVs seamlessly transition to the MPPT mode for full utilization of the solar power at the maximum power point (MPP), i.e.,  $P_{mpp}$ . Consequently, the BSSs become the only power sources to regulate the common DC bus voltage. It is also noted that, apart from the charging/discharging power limits  $P_b^{\min}$  and  $P_b^{\max}$ , the batteries are subject to SoC limits. To preserve battery life, the information of SoCs will be integrated into the BSS droop curves to mitigate overcharging and over-discharging issues, which will be discussed later.

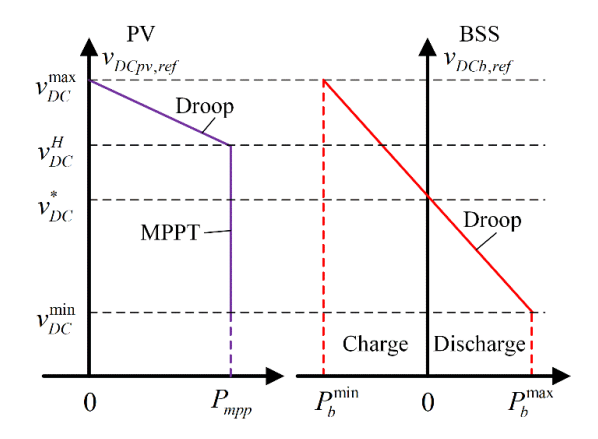


Fig. 1. Droop curves of a PV unit and a BSS unit.

#### A. Adaptive Control for PVs

As shown in Fig. 2, a DC-DC boost converter is employed to interface the PV panel with the DC nanogrid. The cascade control structure consists of three control loops. The V-P droop characteristic in Fig. 1 is realized in the outer loop, which generates the DC bus voltage reference  $v_{DCpv,ref}$ . A first-order low-pass filter is utilized to suppress fluctuation in solar power and to improve system stability.  $P_{pv}$  represents the filtered solar power. The voltage reference for a PV unit is given by:

$$v_{DCpv,ref} = v_{DC}^{max} - R_{d,pv} P_{pv} \tag{1}$$

The droop coefficient  $R_{d,pv}$  is defined as:

$$R_{d,pv} = \frac{P_{mpp}}{v_{DC}^{max} - v_{DC}^H} \tag{2}$$

The intermediate DC bus voltage control loop then acts on  $v_{DCpv,ref}$  and produces the PV voltage reference  $v_{pv,ref}$  for the inner control loop via a proportional-integral (PI) controller with integral clamping and a mode switch block. The duty cycle D to the boost converter is generated in the inner voltage loop using another PI controller. In the proposed PV control scheme, the PV panel is regulated on the left side of the MPP of its P-V characteristic curve in Fig. 3. to facilitate mode switch. The MPP can be estimated off-line by combining the PV module manufacturing parameters with real-time temperature and solar irradiance [16]. In addition, the mode switch block enables a seamless transition between MPPT and droop modes. When the output of the intermediate control loop varies within the range of 0 and  $v_{mpp}$  (the PV voltage at the MPP shown in Fig. 3),

 $v_{pv,ref}$  equals this output, and the PV unit works in the droop mode accordingly. However, the output will increase and  $v_{pv,ref}$  will saturate at  $v_{mpp}$  once the DC bus voltage drops greatly, thus making the PV unit operate in the MPPT mode.

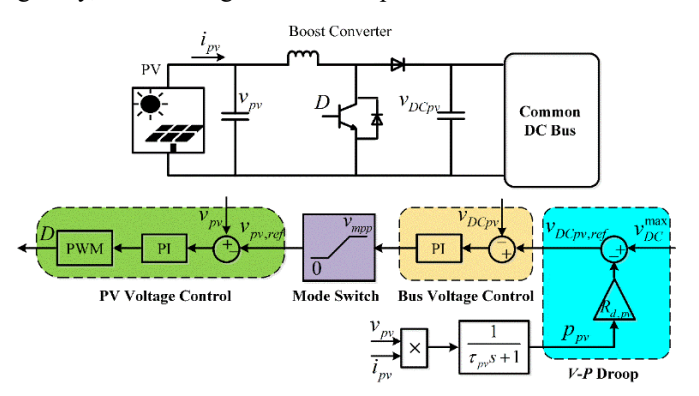


Fig.2. Control diagram of a PV unit.

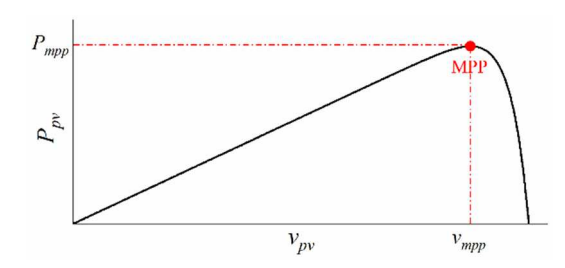


Fig.3. P-V characteristics diagram of a PV panel.

## B. Adaptive Droop Control for BSSs

Bidirectional DC-DC converters should be employed for bidirectional power flow required for BSSs. In this paper, the dual-active-bridge (DAB) DC-DC converter, as shown in Fig. 4, is favored for its advantages such as high power density, high efficiency, and galvanic isolation. Furthermore, the single phase shift (SPS) modulation scheme in [17] is adopted due to its simplicity and effectiveness. Under this scheme, two sets of control signals, i.e., S1 through S4 and Q1 through Q4 for gate drivers of the two H-bridges in Fig. 4 are square waves with a constant duty cycle of 50%. The bidirectional battery power flow  $P_b$  is controlled by regulating the phase shift  $\phi$  between the two sets of control signals.  $P_b$  is positive in the discharging mode and negative in the charging mode. If the lumped leakage resistance  $R_t$  of the high-frequency transformer is ignored, then  $P_b$  can be quantitatively derived as [18]:

$$P_b = \frac{n \cdot v_b \cdot v_{DCb} \cdot \phi}{2\pi \cdot f_{SW} \cdot L_t} \left( 1 - \frac{|\phi|}{\pi} \right) \tag{3}$$

where n is the transformer turns ratio,  $f_{sw}$  is the switching frequency, and  $L_t$  is the leakage inductance of the transformer referred to the battery side. Also,  $v_b$  and  $v_{DCb}$  are the voltages on the battery and DC nanogrid sides, respectively. Equation (3) indicates that  $P_b$  is a parabolic function of  $\phi$  and it has the largest absolute value at  $\phi = \pm \frac{\pi}{2}$  when the voltages are assumed to be constant.

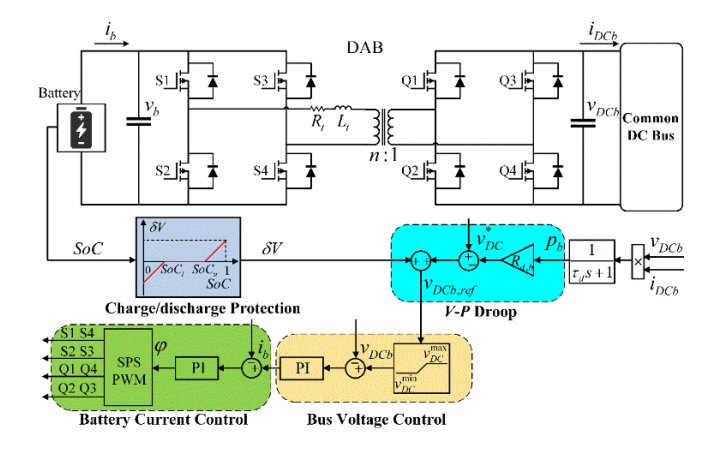


Fig. 4. Control diagram of a BSS unit.

The proposed cascade control structure consists of three control loops. The outer control loop implements the V-P droop characteristic of a BSS unit as shown in Fig. 1, and also takes account of an additional voltage term  $\delta V$ :

$$v_{DCb,ref} = v_{DC}^* - R_{d,b}P_b + \delta V \tag{4}$$

where the droop coefficient  $R_{d,b}$  is defined as:

$$R_{d,b} = \frac{v_{DC}^{max} - v_{DC}^{min}}{P_{b}^{max} - P_{b}^{min}}$$
 (5)

and  $\delta V$  comes from the charge/discharge protection module in Fig. 4, which provides adjustment to the DC bus voltage reference based on a real-time SoC estimation. The SoC estimation could be obtained using several methods [19], and in this work, the coulomb counting method is employed:

$$SoC(t_2) = SoC(t_1) - \frac{\eta}{C_b} \int_{t_1}^{t_2} i_b(\tau) d\tau \tag{6}$$

where  $SoC(t_1)$  and  $SoC(t_2)$  are the SoCs at time instants  $t_1$  and  $t_2$  respectively.  $C_b$  is the battery rated capacity,  $i_b$  is the discharging current, and  $\eta$  is the coulombic efficiency.

Then the modified voltage reference  $v_{DCb,ref}$  to the intermediate bus voltage control loop is bounded between  $v_{DC}^{\min}$  and  $v_{DC}^{\max}$  for reliable operation. The phase shift between the control signals is generated in the inner battery current control loop via a PI controller.

It should be noted that the proposed SoC-based adaptive control could be conveniently embedded into the BSS V-P droop curve via the charge/discharge protection module. To identify the battery overcharge/over-discharge statuses, we denote the upper and lower thresholds of SoC as  $SoC_u$  and  $SoC_l$ , respectively. The protection mechanism is elaborated in the following:

$$\delta V = \begin{cases} R_l(SoC - SoC_l), & SoC \in [0, SoC_l) \\ 0, & SoC \in [SoC_l, SoC_u] \\ R_u(SoC - SoC_u), & SoC \in (SoC_u, 1] \end{cases}$$
(7)

where 
$$R_l = \frac{v_{dc}^* - v_{dc}^{min}}{SoC_l}$$
 and  $R_u = \frac{v_{dc}^{max} - v_{dc}^*}{1 - SoC_u}$ 

When the SoC lies within the normal range  $[SoC_1, SoC_n]$ , charge/discharge protection will not impact the voltage reference. However, the SoC-based adaptive control is enabled when the measured SoC falls outside of this range, as shown in Fig. 5. If the battery is discharging and the SoC decreases below  $SoC_{l}$ , the droop curve then dynamically shifts downwards by  $\delta V$ , lowering the DC bus voltage reference. Therefore, the battery will decrease its discharging power along the translated droop curve until a new steady state is reached. Thus, overdischarging could be mitigated. The trajectory of the changing operating point is illustrated by the red arrows in the left subplot of Fig. 5. Likewise, if the battery is charging and the SoC increases above  $SoC_{ij}$ , the droop curve then shifts upwards by  $\delta V$  as a way of alleviating over-charging. In both cases, the battery power output is regulated by the modified voltage reference. Moreover, if there are multiple BSSs in the nanogrid, their SoCs can tend towards a balance (i.e., similar SoC levels) over time, since the modified voltage reference of the BSS unit with a high SoC is higher and that of the BSS unit with a low SoC is lower.

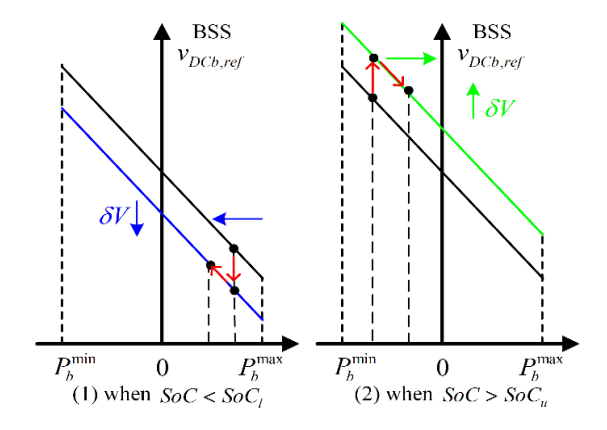


Fig. 5. Curves of SoC-based droop control for two cases.

The proposed control strategies for PV and BSS units are implemented locally, and thus are fully decentralized and only require the measurements of the DC bus voltages, which ensures the plug-and-play function. Besides, they are naturally coordinated via the designed *V-P* droop curves, and can guarantee at least one type of distributed generators is in place to stabilize the common DC bus voltage. Hence, the DC nanogrid system reliability can be improved and control complexity is also decreased.

#### III. SIMULATION RESULTS

The dynamic performance of the proposed DC nanogrid control strategy is validated via MATLAB/Simulink under varying DC loading and solar irradiance conditions. Fig. 6 shows an islanded DC nanogrid test system, which consists of one PV panel, two BSSs, one static load, and one dynamic load.

In the testing system, the nominal value of the common DC bus voltage  $(v_{DC}^*)$  is 380 V, while its permissible limits  $v_{DC}^{\max}$  and  $v_{DC}^{\min}$  are 405 V and 355 V, respectively. The high voltage value  $v_{DC}^H$  is set as 390 V empirically. For simplicity, the

coulombic efficiency of 100% is assumed for the BSS units.  $SoC_u$  is set as 0.8, while  $SoC_l$  is 0.3. Furthermore, the initial SoCs of BSS 1 and BSS 2 are set as 0.79951 and 0.30003 respectively to demonstrate the effectiveness of the proposed charge/discharge protection mechanism. Since the battery dynamics are usually slow, the coefficients  $R_l$  and  $R_u$  calculated in (7) are also augmented by 400 times to strengthen the effectiveness for limited simulation time. For the PV unit, its cell temperature is assumed to be 25 ° C throughout the simulation with the solar irradiance variation shown in Fig. 7, and the dynamic load is shown in Fig. 8. Controller parameters are obtained from small-signal stability analysis and are provided in the Appendix along with other system parameters.

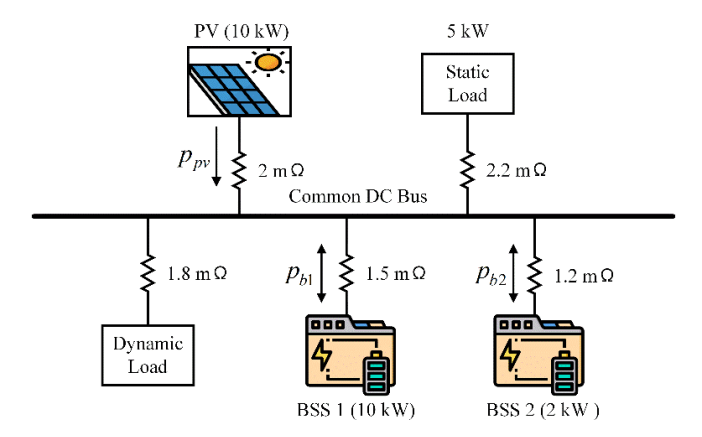


Fig. 6. Topology of an islanded DC nanogrid test system.

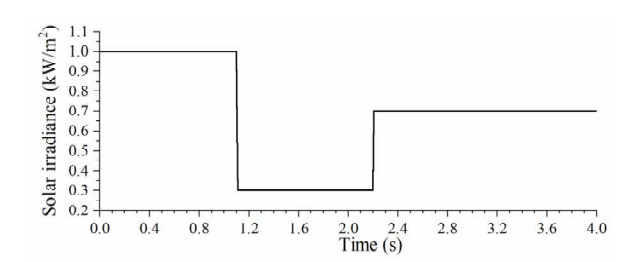


Fig. 7. Solar irradiance curve.

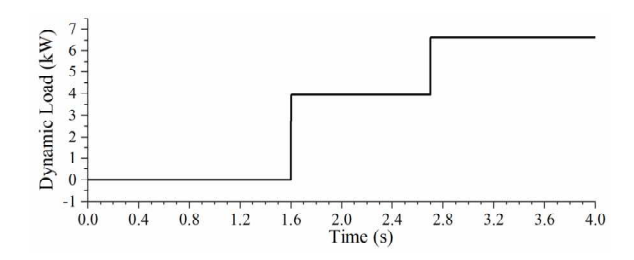


Fig. 8. Dynamic load curve.

The DC bus voltages measured at the output terminals of the three distributed generators are presented in Fig. 9. It can be observed that the voltages almost coincide and that they are all well-regulated within the permissible voltage range. Initially, the common DC bus voltage stays at around 391 V, slightly above  $v_{DC}^H$ . Hence, the PV unit limits its power output and generates 9.217 kW as opposed to 9.958 kW at MPPT, as shown

in Fig. 10. As the common DC bus voltage is high enough, both BSSs operate in the charging mode.

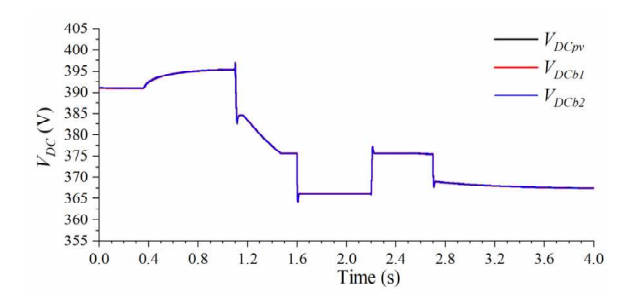


Fig. 9. DC bus voltages of the BSS and PV units.

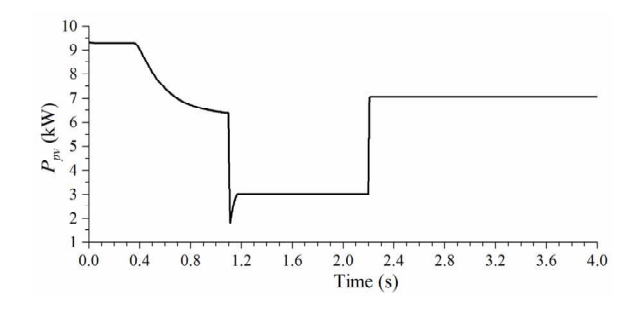


Fig. 10. Power output of the PV unit.

Fig. 11 illustrates the power outputs and the SoCs of the two BSS units over the simulation horizon.

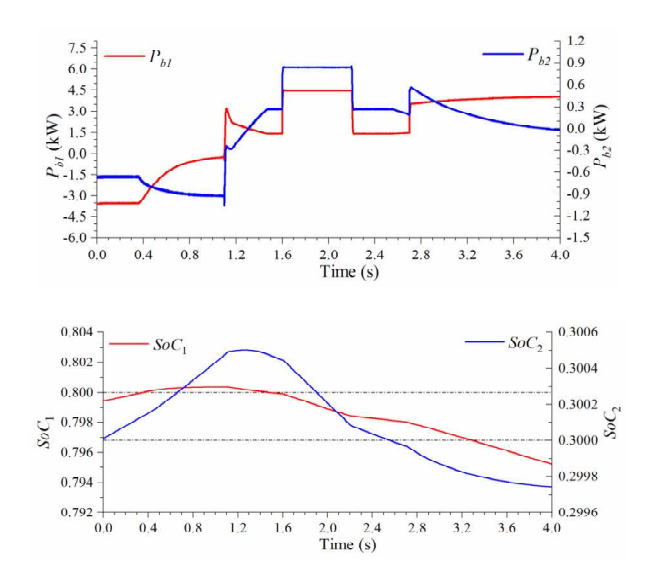


Fig. 11. Power outputs and SoC levels of BSS 1 and BSS 2.

It can be observed that the actual powers shared between the BSS units at steady states are directly proportional to their battery power ratings. At the beginning, both BSS units are charged at constant powers, thereby absorbing excess solar power injecting into the DC nanogrid. At t = 0.37 s, the SoC of BSS 1 rises beyond 0.8, and the charge protection mechanism is triggered. The voltage reference of BSS 1 is thus adaptively raised according to (7). As a consequence, BSS 1 decreases its

charging power and its SoC starts to experience a much slower increase. Meanwhile, BSS 2 begins to pick up more charging power and its SoC level is still within the normal range. Due to the increase in the DC bus voltage, the PV unit provides less power as per its *V-P* droop characteristic curve, as shown in Fig. 10. But the PV unit still participates in voltage regulation along with the BSSs.

As the solar irradiance plunges at t = 1.1 s, the common DC bus voltage sees a significant decrease, and the PV unit is forced to operate in the MPPT mode after a small transient and yields 3.016 kW at a new steady state. During this process, both BSS units are discharging to supply more power to compensate for the instantaneous power imbalance, and also to regulate the common DC bus voltage. From t = 1.6 s to t = 2.2 s, the DC nanogrid experiences the highest net load (i.e. the total electrical demand minus the solar power generation), which is reflected by the largest decreasing rates of the BSS units' SoCs. It should be noted that as the solar irradiance increases after t = 2.2 s, the PV unit still operates in the MPPT mode, delivering the highest solar power available due to the low DC bus voltage. In the meantime, the two BSS units continue discharging to provide power support and voltage regulation. When t = 2.56 s, the SoC of BSS 2 begins to fall below 0.3, thus automatically triggering the discharge protection mechanism. As a result, the DC bus voltage reference of BSS 2 is reduced according to (7). BSS 2 then generates far less power and sees a slowdown of its SoC decline. On the other hand, BSS 1 still operates within its normal SoC range and fulfils virtually all the electrical demand afterwards. It is possible that both BSS units hit their lower SoC thresholds and are thus no longer able to power the loads. In this extreme case, load shedding will be performed.

The simulation results exhibit good dynamic performance of the proposed coordinated control strategy, and the control system is stabilized well. As the DAB topology facilitates the bidirectional power flow of the BSS units, the phase shifts generated by the inner battery current control loop are also presented in Fig. 12. The sign of the phase shifts indicates whether the BSSs are in charging or discharging modes. Smooth transition between charging and discharging switching is achieved during the entire simulation. Interestingly, the phase shift curves of BSS units look very similar to those of their power outputs as shown in Fig. 11. The reason is that the two BSS units are operating with phase shifts far away from the extrema  $\pm \frac{\pi}{2}$ , lying in an approximately linear region of the parabolic function.

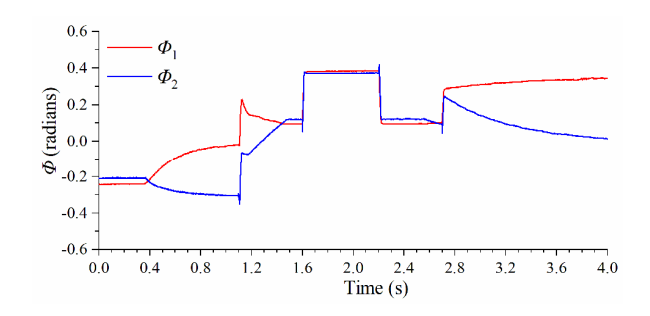


Fig. 12. Phase shifts generated for BSS 1 and BSS 2.

#### IV. CONCLUSIONS AND FUTURE WORK

A fully decentralized coordination strategy for controlling the PV-BSS systems in the islanded DC nanogrids has been presented in this paper. The proposed control strategy relies only on the measurements of local DC bus voltages, thus demanding minimum communication capabilities. The PV unit is able to provide power and regulation support to the DC bus voltage by seamlessly switching between the MPPT mode and the droop mode. In addition, an SoC-based adaptive droop control method is proposed for the BSS units that are interfaced by DAB DC-DC converters to regulate the DC bus voltages. Overcharging and over-discharging protection is achieved via the proposed SoC-related voltage control. Simulation results based on MATLAB/Simulink demonstrated good dynamic performance and stability of the proposed coordinated control strategy.

Recognizing that droop control may inevitably cause a deviation from the nominal value of the common DC bus voltage. As a next step, we plan to design a secondary distributed event-triggered approach for DC nanogrids to restore the common DC bus voltage to the nominal value with considerably reduced communication burdens.

## APPENDIX TABLE I. PARAMETERS OF THE BSS UNITS

Parameters	BSS 1	BSS 2
Battery nominal voltage	51.6 V	51.2 V
Battery's P <sub>bmax</sub>	8 kW	1.5 kW
Battery's P <sub>bmin</sub>	-8 kW	-1.5 kW
DAB rated power output	10 kW	2 kW
Transformer's R <sub>t</sub>	2 mΩ	5 mΩ
Transformer's $L_t$	2.85 μΗ	14.25 uH
Transformer's turns ratio n	1/8	1/8
Switching frequency $f_{sw}$	10 kHz	10 kHz
Droop coefficient $R_{d,b}$	3.1 V/kW	16.7 V/kW
Low-pass filter time constant $\tau_d$	0.001 s	0.001 s
Bus voltage controller	8.57 + 2760/s	4.52 + 1310/s
Battery current controller	11.9/s	59.6/s

TABLE II. PARAMETERS OF THE PV UNIT

Parameters	PV
$v_{mpp}$ in Standard Test Conditions	122.8 V
P <sub>mpp</sub> in Standard Test Conditions	9.958 kW
Boost converter's inductance	2.5 mH
Boost converter's output capacitance	1 mF
Low-pass filter time constant $\tau_{pv}$	0.002 s
Bus voltage controller	0.21 + 107/s
PV voltage controller	0.69 + 50/s

## REFERENCES

- [1] M. di Piazza, M. Luna, M. Pucci, G. La Tona, and A. Accetta, "Electrical storage integration into a DC nanogrid testbed for smart home applications," in 2018 IEEE Int. Conf. on Environment and Electrical Engineering (EEEIC), June 2018.
- [2] T Nguyen, JM Guerrero, and G Griepentrog, "A self-sustained and flexible control strategy for islanded DC nanogrids without communication links," *IEEE Journal of Emerging and Selected Topics in Power Electronics.*, vol. 8, no.1, pp. 877-892, March 2020.

- [3] O. Lucia, I. Cvetkovic, H. Sarnago, D. Boroyevich, P. Mattavelli, F. C. Lee, "Design of home appliances for a DC-based nanogrid system: an induction range study case," *IEEE Journal of Emerging and Selected Topics in Power Electronics*, vol. 1, no. 4, pp. 315-326, December 2013.
- [4] S. Aznavi, P. Fajri, A. Asrari, and F. Harirchi, "Realistic and intelligent management of connected storage devices in future smart homes considering energy price tag," *IEEE Transactions on Industry Applications*, vol. 56, no. 2, pp. 1679-1689, March-April 2020.
- [5] H. Elfeqy, A. S. Al-Rumaihi, M. S. Shahin, A. M. Massoud, and A. Gastli, "Design of a low voltage DC grid interfacing PV and energy storage systems," in 2017 IEEE Symposium on Computer Applications & Industrial Electronics (ISCAIE), April 2017.
- [6] M.Yaqoob, M. Nasir, J. C. Vasquez, and J. M. Guerrero, "Self-directed energy management system for an islanded cube satellite nanogrid," in 2020 IEEE Aerospace Conference, March 2020.
- [7] H. W. Yan, A. Narang, H. D.Tafti, G. G. Farivar, and J. Pou, "Reduced battery usage in a hybrid battery and photovoltaic stand-alone DC microgrid with flexible power point tracking", in 2020 IEEE Energy Conversion Congress and Exposition (ECCE), October 2020.
- [8] D. Xu, A. Xu, C. Yang, and P. Shi, "A novel double-quadrant SoC consistent adaptive droop control in DC microgrids," *IEEE Transactions* on Circuits and Systems II: Express Briefs, vol. 67, no. 10, pp. 2034-2038, October 2020.
- [9] D. Li and C. N. M. Ho, "Decentralized PV-BES coordination control with improved dynamic performance for islanded plug-n-play DC microgrid," *IEEE Journal of Emerging and Selected Topics in Power Electronics* (early access), 2020.
- [10] S. Sahoo, S. Mishra, S. Jha, and B. Singh, "A cooperative adaptive droop based energy management and optimal voltage regulation scheme for DC microgrids," *IEEE Transactions on Industrial Electronics*, vol. 67, no. 4, pp. 2894-2904, April 2020.
- [11] H. Cai, J. Xiang, W. Wei, and M. Z. Q. Chen, "V-dp/dv droop control for PV sources in DC microgrids," IEEE Transactions on Power Electronics, vol. 33, no. 9, pp. 7708-7720, September 2018.
- [12] H. Cai, J. Xiang, and W. Wei, "Decentralized coordination control of multiple photovoltaic sources for DC bus voltage regulating and power sharing," *IEEE Transactions on Industrial Electronics*, vol. 65, no. 7, pp. 5601-5610, July 2018.
- [13] W. C. Chan, M. Armstrong, D. Atkinson, and V. Pickert, "V-dP/dI droop control technique with d<sup>2</sup>P/dI<sup>2</sup> to improve steady state performance for multiple PV modules in a dc microgrid," in 2019 21st European Conference on Power Electronics and Applications (EPE '19 ECCE Europe), Septermber 2019.
- [14] S. Augustine, M. K. Mishra, and N. Lakshminarasamma, "A unified control scheme for a standalone solar-PV low voltage DC microgrid system with HESS," *IEEE Journal of Emerging and Selected Topics in Power Electronics*, vol. 8, no. 2, pp. 1351-1360, June 2020.
- [15] Y. Xia, M. Yu, P. Yang, Y. Peng, and W. Wei, "Generation-storage coordination for islanded DC microgrids dominated by PV generators," *IEEE Transactions on Energy Conversion*, vol. 34, no. 1, pp. 130-138, March 2019.
- [16] J. Bai, S. Liu, Y. Hao, Z. Zhang, M. Jiangc, and Y. Zhang, "Development of a new compound method to extract the five parameters of PV modules," *Energy Conversion and Management*, vol. 79, pp. 294-303, March 2014.
- [17] N. Hou and Y. Li, "Communication-free power management strategy for the multiple DAB-based energy storage system in islanded DC microgrid," *IEEE Transactions on Power Electronics*, vol. 36, no. 4, pp. 4828-4838, April 2021.
- [18] T. L. Nguyen, G. Griepentrog, and V. T. Phung, "Modeling and control of dual active bridge converter with two control loops and output filter," in ECON 2017-43rd Annual Conference of the IEEE Industrial Electronics Society, October-November 2017.
- [19] G. S. Misyris, D. I. Doukas, T. A. Papadopoulos, D. P. Labridis, and V. G. Agelidis, "State-of-charge estimation for li-ion batteries: a more accurate hybrid approach," *IEEE Transactions on Energy Conversion*, vol. 34, no. 1, pp. 109-119, March 20